**FOREIGN**
**BROADCAST**
**INFORMATION**
**SERVICE**

# *JPRS Report*

# Science & Technology

## *Japan*

16TH COMPOSITE MATERIALS SYMPOSIUM

# SCIENCE & TECHNOLOGY

## JAPAN

## 16TH COMPOSITE MATERIALS SYMPOSIUM

926C0017 Tokyo FUKUGOZAIRYO SYMPOSIUM in Japanese Oct 91 pp I-XXVIII, 1-130

[Selected papers from the proceedings of the 16th Composite Materials Symposium held 14-15 Oct 91 in Fukuoka City, sponsored by the Japan Society for Composite Materials]

## CONTENTS

Development of Al Preform-Wire Reinforced by SiC Fiber

[Article by Y. Imai, et al., Nippon Carbon Company, Ltd.]

[Text]   1.   Purpose

The principal causes for the delay in the popularization of fiber-reinforced metals (FRM's) are the difficulty in manufacturing them, and their high cost, which is especially true for long fiber types.  The basic technologies required for manufacturing FRM's are composing and shaping, and forming methods.  These must be able to satisfy both requirements simultaneously, and it must be said that there are only a very few such techniques.  Therefore, if one treats composing and shaping separately, then shaping needs to be performed only as a post-process, provided that there are preforms that already have been composed.  As a result, the selection of applicable forming methods and the degree of freedom for the size and shape of the compacts can be increased markedly.  For this reason, we set out to develop already composed wire-shaped preforms as the most basic material form.

2.   Method

In our study we adopted a continuous SiC fiber manufactured using domestic technology (trade name: Nicalon) as the reinforcing fiber, and Al system wires as the matrix.  Since this is a continuous fiber with a small diameter (14 µm) and multiple fiber types (500 lines/yarn), the important point of the technology is to uniformly orient the metal in the numerous gaps between fibers.  For this reason, we employed the continuous molten metal penetration method, which we anticipate will provide high efficiency and consistent quality.

The process can be summarized as follows.  First, it is necessary to ensure defiberability by removing the sizing agent (collecting agent).  Next, molten Al is allowed to penetrate completely into the gaps between the fibers to be compounded, and then the compounded fibers are wound on a drum by continuously pulling them up through a nozzle.

The wire thus obtained was subjected to tensile tests at room temperature and at high temperatures.  The fractured surface and the fine structures were then examined by a scanning electron microscope (SEM), etc.

## 3. Results and Considerations

We found that it was effective to reduce the temperature of the molten metal as much as allowable by the operation, and to increase the threading speed in order to suppress interface reactions. The increase in the fiber volume fraction (Vf) for improving the strength was attained by reducing the nozzle diameter. This made it possible to obtain a high level of strength that conforms to the rules of mixing (ROMs) for a range of about 0.3 to 0.5 for Vf. Table 1 shows representative properties. It can be seen that these light-weight samples have excellent specific strength and specific rigidity compared to conventional structural materials. From Figure 1, which shows the high-temperature properties, it also can be seen that they have excellent strength at high temperatures compared to Al or Ti alloys. No decrease in strength at room temperature after high-temperature treatment was observed, although there is a drop in the strength of the SiC/pure Al system in high temperature region. We believe this was due to the plastic deformability of the matrix at high temperatures, and the heat resistance of the matrix was improved. In other words, to ensure that we used an extremely rational method for molten metal penetration, we selected an Al-5.7Ni alloy composite, which is a unidirectionally solidified eutectic alloy. This is a so-called "in-situ composite" in which an ultrafine fibrous $Al_3Ni$ intermetallic compound is formed densely in the $Al-Al_3Ni$ eutectic phase, filling the gaps between the SiC and the fiber. The results are shown in Figure 2 [photo not reproduced]. The Al-Ni system held its room temperature strength even at 450°C, as can be seen from Figure 1.

Table 1. Representative Properties of SiC (Nicalon)/Al Preform

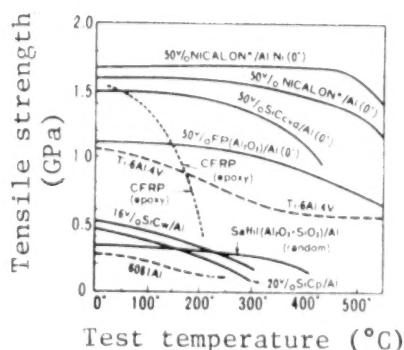| Item | Property | |
|---|---|---|
| Cross-sectional shape | Circular | Circular |
| Outer diameter | 0.5 mm | 0.3 mm |
| Fineness | 500 g/1,000 m | 170 g/1,000 m |
| Tensile strength | 1,200 MPa | 1,500 MPa |
| Tensile modulus of elasticity $E_1$ | 130 GPa | 140 GPa |
| $E_2$ | 80 GPa | 85 GPa |
| Vf | 45 Vol% | 50 Vol% |
| Minimum diameter of bending | 30 mm | 20 mm |



Figure 1. Comparison of High-Temperature Tensile Strength of Various Al-System FRM's

We attempted FRM formation using a preform wire as an intermediate material. Since the reinforcing fiber has a fine diameter and is flexible, hot pressing made it possible to obtain curved materials and bent materials in addition to plates. Long sheets were obtained by hot rolling, raising the possibility that these could be used for beam materials, etc. Using HIP it was possible to form pipe materials as trial profiles. Next, FRM's were formed by obtaining a preform wire. Figure 3 [photo not reproduced] shows cylinder blocks for an on-vehicle air conditioner as an example. These were obtained by die casting and by orienting wires in pipe form only for the cylinder parts that require reinforcement.

From what has been described above, it can be said that it may be possible to overcome the various problems -- difficulty in forming complicated shapes and large materials, low productivity, high cost, etc. -- which up to now have obstructed the practical use of FRM's.

4. Conclusions

(1) It proved possible to manufacture wire-form composites where Al is reinforced by continuous SiC fibers (Nicalon) by the molten metal penetration method. Under the proper conditions, it proved possible to obtain reinforcing fibers with sufficient strength.

(2) In order to improve the heat resistance, an in-situ unidirectionally solidified eutectic alloy, Al-Ni system, was employed as the matrix. Wires showed no deterioration of strength even at 450°C when the matrix was of the fiber-reinforced type.

(3) Evaluations of the developed wires showed that it was possible to form various kinds of FRM's by various forming methods.

Properties of Long Fiber-Reinforced Thermoplastics

[Article by M. Koshimoto, et al., Idemitsu NSG Company, Ltd. and Kyoto Institute of Technology]

[Text]  1.  Introduction

Materials for press forming that are obtained by reinforcing thermoplastic resins with long glass fiber mats are generally called stampable sheets. These materials recently have been attracting attention because the use of thermoplastic resins as the base matrices may make it possible to use them on a recycling basis.  A stampable sheet is a laminated metal obtained by heating, melting, and impregnating a thermoplastic resin into long glass fiber (GF) mats.  These mats possess such features as excellent specific strength and specific rigidity, and they also have a short formation cycle. Since, however, the mechanical properties of compacts after press formation depend greatly on the fibers used as the reinforcing materials, it is necessary to understand their fluidic behavior, fiber orientation, fiber content fraction, etc., which in turn depend on the constitution and formation conditions of the materials.

In the past, we have investigated the effect of the temperature of the material at the time of formation on the nonuniformity of the bending characteristic of the compact.  Also, we have sought to understand the flow of the glass fiber and the resin in the various laminated layers through the use of a unique technique in order to observe the flow state of the material.  As a result, we found that the flow of the material charged to the die at the time of formation is faster toward the central part in the thickness direction, and that the fiber at the central part flows to the outer periphery and is oriented along the die.  Meanwhile, there is a large deviation in the distribution of the fiber in the part where the material is charged, and in the part where the material has flowed at the time of formation.  In particular, it was found that there are formed portions where the fiber distribution is low in the periphery of the charge, and this in turn creates nonuniformity in the mechanical properties.  As a method for resolving this difficulty, we have been proposing that it is effective to keep the temperature of the material low in the central layer, which is charged at the time of formation, to suppress the flow of the material at the central part in order to obtain a uniform flow in the respective layers.

4

In the present study, we sought to achieve uniformity in the mechanical properties of the compact as a whole by paying attention to the length of the glass fibers that constitute the GF mats as a factor governing the flow of the glass fibers at the time of press forming. In addition, we also investigated the effect of the heating temperature. Since the continuous glass fibers are intertwined three-dimensionally by the needle punching process in the ordinary GF mat, the flow of the glass fibers is constrained. For this reason, we manufactured laminated materials that were reinforced with chopped strands whose fiber length is controllable and that were less intertwined with the glass fibers. We then conducted an experiment to compare the materials that have GF mats.

2.  Samples and Forming Conditions

The sample used in the experiment was a stampable sheet made by Idemitsu NSG Company, Ltd. (trade mark: X sheet). This is a laminated material reinforced by GF mats with a randomly oriented polypropylene base matrix. In addition, laminated materials reinforced by chopped strands were used in order to examine the influence of the glass fiber length on the flow behavior at the time of formation and the mechanical properties of the compacts. We used chopped strands of three different lengths -- 50, 25, and 13 mm. The composition of the laminated material was 19 percent by volume glass fibers and 81 percent by volume polypropylene. The material was adjusted to produce a plate thickness of 3.8 mm for the original cloth.

The die used for forming was a plate forming die 300 mm x 300 mm. The dimensions of the material, and the number of layers to be laminated, were selected so that a plate thickness of 3.8 mm for the compact could be obtained. The charging position of the heated material by the heater in the die was in the central part of the die. The charging factor was 33 percent, and there were three laminated layers, as shown in Figure 1. A far infrared heater was used to heat the material, and the temperature at the central part of the raw material was set at either 180° or 200°C by varying the heating time. The general heating temperature at the time of press forming was 200° ± 10°C, but the temperatures of the various layers at the time of charging in the die, and the length of glass fiber of the material were varied as shown in Table 1. First, we examined the effect of the fiber length (LF = 50, 25). Next, we investigated the effect of the fiber length when the flow of the second layer was suppressed by heating temperatures (LFT = 50T, 25T), that is, the case of suppressing the flow of the second layer in order to increase the flow of the first and the third layers. Since little change in the flow resistance was observable for temperatures above 200°C, chopped strands of 25 mm were used (252) to increase the flow of the first and the third layers, and chopped strands of 13 mm were used (151) to increase the flow of the first and the third layers. Figure 2 shows the tensile and the bending characteristics of the materials used in this experiment as functions of the length of the glass fibers.

The conditions for press forming were as follows: forming pressure = 150 kg/cm$^2$, pressurizing speed = 7.5 mm/sec, die temperature = 50°C, and holding time at pressurized cooling = 30 sec.
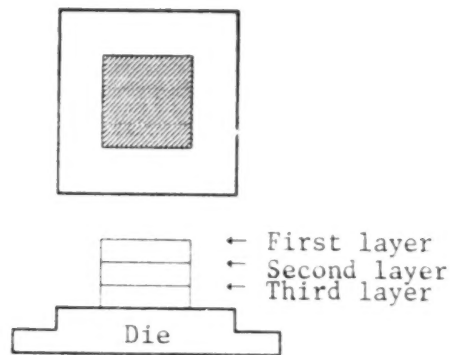
5

Figure 1. Charging Position in the Die

Table 1. Glass Fiber Lengths and Heating Temperatures for Various Layers at the Time of Forming

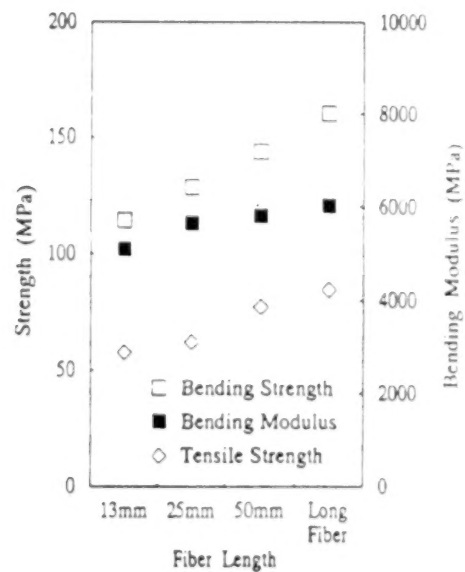| Type | | LF | 50 | 25 | LFT | 50T | 25T | 252 | 151 |
|---|---|---|---|---|---|---|---|---|---|
| Heating temperature | First layer | 200°C | | | 200°C | | | 200°C | |
| | Second layer | | | | 180°C | | | | |
| | Third layer | | | | 200°C | | | | |
| Glass fiber length | First layer | GF mat long fiber | 50 mm | 25 mm | GF mat long fiber | 50 mm | 25 mm | 25 mm | 13 mm |
| | Second layer | | | | | | | 50 mm | 50 mm |
| | Third layer | | | | | | | 25 mm | 13 mm |



Figure 2. Relationship Between Glass Fiber Length and Mechanical Properties

6

## 3. Experimental Method

In order to evaluate the bending property of various parts of the compact obtained by press forming, test pieces were segmented from positions as shown in Figure 3. The dimensions of the test pieces were 80 mm x 15 mm x 3.8 mm. The test conditions were as follows: cross head speed = 3 mm/min, span length = 63 mm, and indentator radius = 5 mm. The bending modulus and the bending strength were determined by a three-point bending test that uses an autograph, and the glass fiber content was measured from a test piece that was tested by the ashing method.
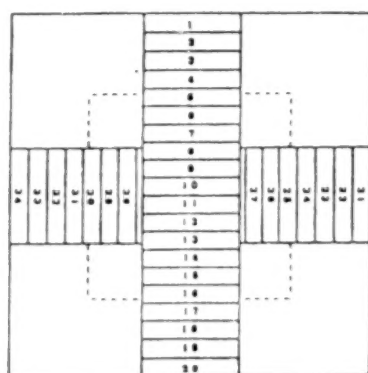


Figure 3. Test Piece Acquiring Positions

## 4. Results and Considerations

Since the compact is a square laminated plate, the evaluation of all test pieces was carried out by making them to correspond to test pieces with test piece numbers 1 to 10. The bending test enabled us to evaluate the relationship between bending strength and the bending modulus, and the results are shown in Figure 4. Since there is a good correlation between the bending strength and the bending modulus for laminates with various fiber lengths, we decided to compare our results against the bending modulus. The changes in the bending modulus for the case of formation by heating each layer to 200°C corresponding to the general formation condition are shown in Figure 5. The nonuniformity of the bending modulus at various positions in the plate for various values of the length of the glass fibers of the material showed similar tendencies, revealing a decrease in the bending modulus at the periphery of the charge (test piece numbers 3 and 4). This is due to the decrease in the glass fiber fraction shown in Figure 6. In contrast, in the case of formation with a low heating temperature of 180°C for the second layer, as shown in Figure 7, the decrease in the bending modulus in the charge periphery can be suppressed, but observation of the flow reveals that what is flowing to the peripheral edges of the compact is only the resin of the second layer, which sharply reduces the fiber fraction at the peripheral edges of the compact. As a result, a marked reduction in the bending modulus is observed at the peripheral edges of the compact. A comparison of the effect of fiber length shows that there exists a tendency toward less

7

nonuniformity in the bending modulus for smaller fiber lengths. Figure 9 shows the nonuniformity of the bending modulus for the case of formation by lamination of materials with different fiber lengths. When a compact is formed by laminating materials with a fiber length of 50 mm for the second layer, and 13 mm for the first and the third layers (case 151), the bending modulus at various parts of the compact is approximately uniform, and the nonuniformity in the fiber fraction also is satisfactory, as shown in Figure 10. For this lamination structure, we learned through the use of a unique technique of flow observation that the flow of glass fibers with a smaller length in the first and the third layers is greater than the flow in the second layer, with an overall dispersion of the glass fibers in the first and the third layers throughout the entire compact. We believe that the reduction of nonuniformity of the mechanical properties can be attributed more to the uniform flow of the fibers in each layer than to the low heating temperature of the second layer with uniform dispersion of the glass fibers.
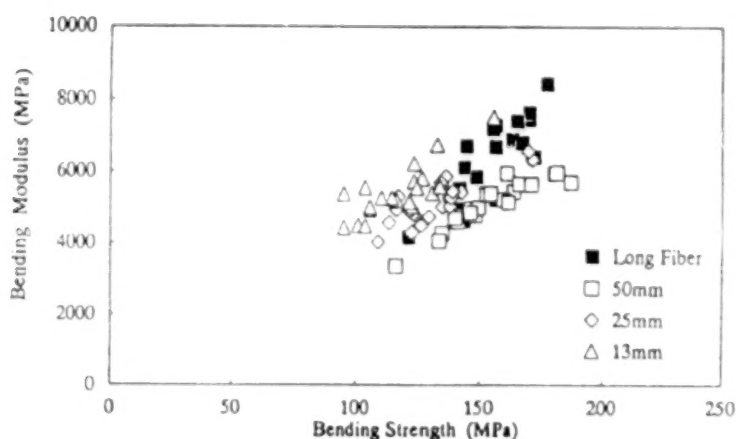


Figure 4. Relationship Between Bending Strength and Bending Modulus
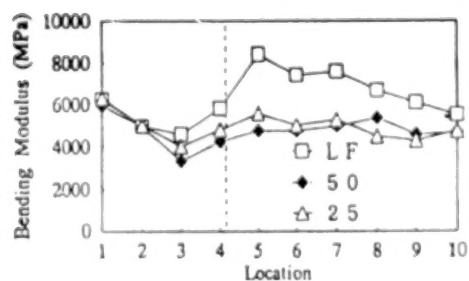


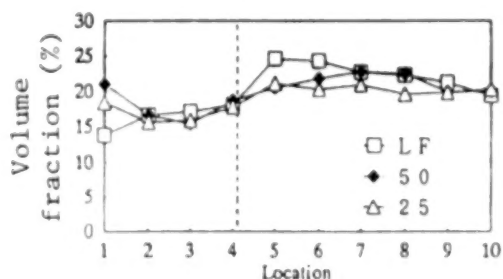Figure 5. Relationship Between Test Piece Acquisition Position and Bending Modulus

Figure 6. Relationship Between Test Piece Acquisition Position and Glass Fiber Volume Fraction
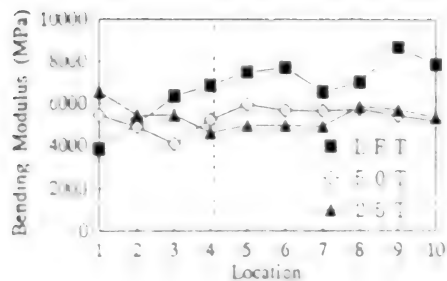
8

Figure 7. Relationship Between Test
Piece Acquisition Position and
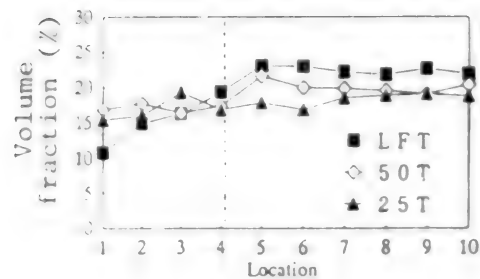Bending Modulus



Figure 8. Relationship Between Test
Piece Acquisition Position and
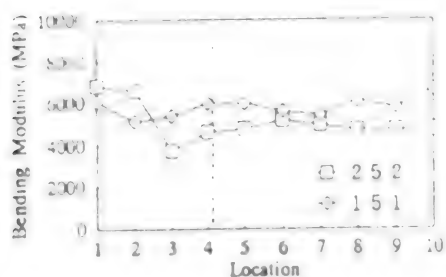Glass Fiber Volume Fraction



Figure 9. Relationship Between Test
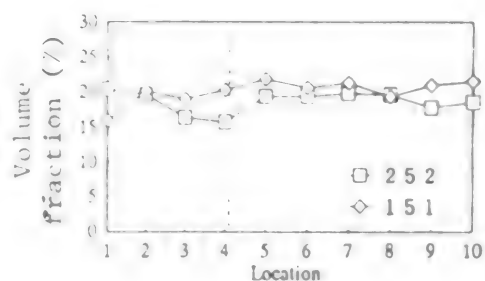Piece Acquisition Position and
Bending Modulus



Figure 10. Relationship Between Test
Piece Acquisition Position and
Glass Fiber Volume Fraction

Strength, Toughness of Multiaxial Reinforced 3D Composites

[Article by Shu Yamashita, et al., Materials and Electronic Device Laboratory, Mitsubishi Electric Corporation]

[Text]   1.   Introduction

Accompanying the increasingly diverse applications of composite materials is a growing need for three-dimensional material design.  For structural materials, particular problems include the generation of multiaxial stress and the increasingly complex shapes that accompany their use as primary structural members.  For functional materials, one must consider control of the materials' three-dimensional thermal properties, and their electromagnetic properties.

In this paper, we will report the results of our investigation of the compressive strength and the fracture toughness of seven-axial reinforced three-dimensional (7A3D) composites in order to acquire basic data and to clarify the fracture behavior of multiaxial reinforced three-dimensional (MA3D) composites.

2.   Manufacture of Specimens

Table 1 shows the reinforcements and matrices used for the manufacture of the specimens.  Also included in the table for the purpose of comparison is information on three-axial and four-axial reinforced three-dimensional (3A3D and 4A3D) composites that have been reported already.  In 7A3D's, rod-piercing formation base materials similar to those for 4A3D's are being used. The impregnation of resin into the formation base material was done by means of a vacuum impregnation method, and curing was carried out at ordinary temperature.

3.   Evaluation Test

3.1   Specimen

Figure 1 presents three schematic diagrams of concepts for the orientation of reinforcement for 3A3D, 4A3D, and 7A3D.  In the figure, each cube represents

a unit structure.  The solid lines represent the orientation direction of the reinforcement; broken lines represent the direction of stress on the test pieces, which are designated as Type A and Type B.  We made separate test pieces for compression tests and for fracture toughness tests, as shown in Figure 2.

Table 1.    Reinforcements and Matrices

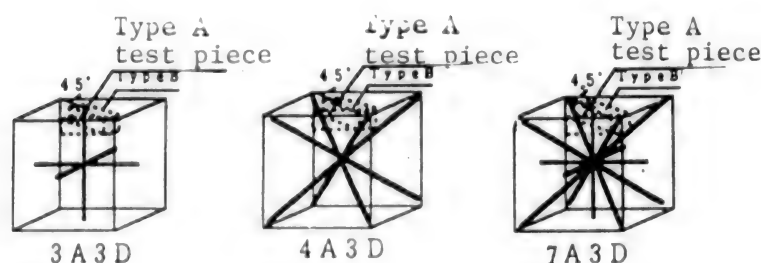| | 3A3D | 4A3D | 7A3D |
|---|---|---|---|
| Reinforcement | CF-fabric<br>Fiber : Toray,<br>T300-12kfila. | CFRP-rod<br>Fiber : Toray, T-300<br>Matrix : polyester<br>Vf : 60%<br>Diameter: 0.77mm | |
| Matrix | Epoxy resin | | |
| $V_f$ (%) | 40,  49 | 40 | 34 |



Figure 1.    Concept for Reinforcement Orientation



Compression test          Fracture toughness
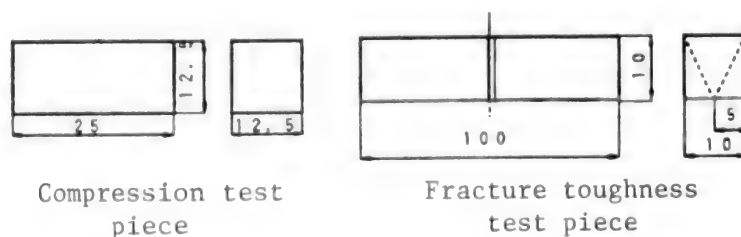piece                      test piece

Figure 2.    Test Piece Dimensions

## 3.2   Testing Method

For the tests we used an instron-type universal material testing machine (Model 1185).  The cross-head speed was 0.5 mm/min.  The strength in the compression test was determined by loading to the ultimate fracture after determining the elastic modulus and the Poisson ratio by means of a strain gauge.  The fracture toughness was determined by work of fracture (WOF) by a three-point bending test using a chevron-notched test piece.  The WOF is the amount of work per unit cross-sectional area applied to a test piece from the outside.  It is calculated by dividing the amount of work corresponding to the surrounding area by the load-displacement curve and

11

the displacement axis by twice the projected cross-sectional area of the
fracture surface.

4.   Experimental Results

4.1   Compression Test

The measurements of the compressive modulus of elasticity are shown in
Figure 3.   In the figure, the values for 3A3D's and 4A3D's have been
extracted from past reports, and the abscissa represents the fiber volume
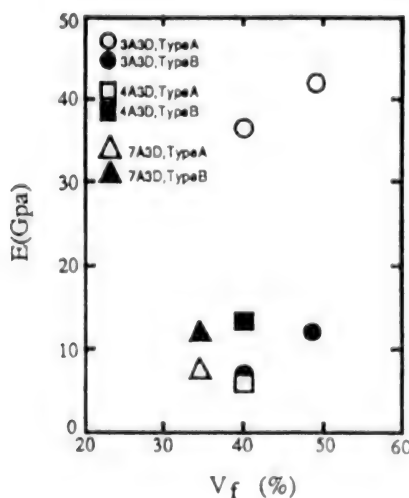f.action.



Figure 3.   Compressive Modulus of Elasticity of MA3D's

A theoretical analysis that makes the modulus of elasticity of a 7A3D to be
more three-dimensionally isotropic has been reported.   Our measurements also
showed considerable isotropy compared to 3A3D's or 4A3D's.   Although a low
elasticity reinforcement was employed in this experiment, it is possible to
obtain materials with a high specific rigidity and high specific strength
having less three-dimensional anisotropy by manufacturing 7A3D's with highly
elastic reinforcements.

Figure 4 shows representative load-displacement curves from the compression
test.   As can be seen from Figure 1, the orientation directions of the
reinforcements in the 7A3D are a combination of those for 3A3D's and 4A3D's,
and the fracture behavior also showed a situation that is consistent with
this consideration.   In other words, microbuckling of the rod parallel to
the direction of the load is dominant in the fracture behavior of the 3A3D
Type A test piece, while deformation in the mutually obliquely oriented rods
with respect to the direction of the load is dominant in the fracture behavior
in the 4A3D Type A test piece.   In the 7A3D Type A test piece, after an
elastic deformation in Region 1, microbuckling occurs in the reinforcement
parallel to the load direction, and cracks appear in the matrix (Region 2).
There also is a deformation due to the four axes of the reinforcements that

12

are obliquely oriented (Region 3). Finally, microbuckling or bending frac-
tures are generated in the four axes that are deformed by the constraints of
the reinforcements that are oriented perpendicular to the load direction
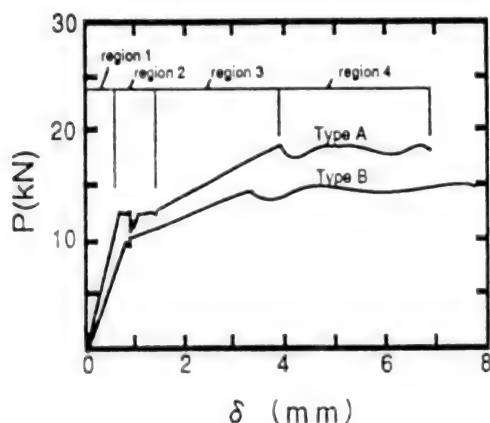(Region 4).



Figure 4.   Representative Load-Displacement Curves

In contrast, in the Type B test piece there are no reinforcements that are
parallel to the load direction.  Thus, after elastic deformation, fracturing
proceeded to the deformation of the obliquely oriented reinforcements, without
observing Region 2.

The compressive strength of the 7A3D's as well as that of the 3A3D's and the
4A3D's are shown in Figure 5.  Analogous to the results for the modulus of
elasticity, the difference between Type A and Type B is small, and there
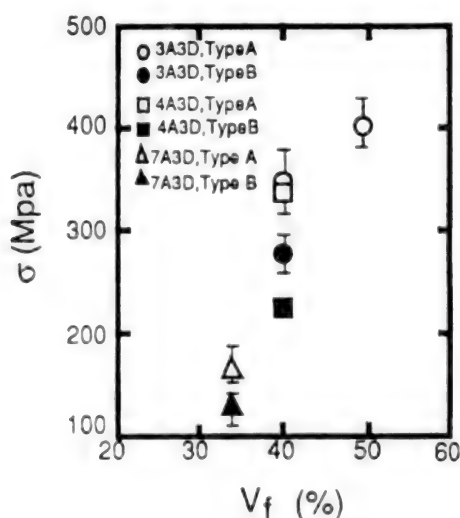exists no anisotropy of the characteristics in the 7A3D's.



Figure 5.   Compressive Strength of MA3D's

13

## 4.2  Fracture Toughness Test

In the Type A test piece, unstable fissure progress due to bending fractures in the reinforcement oriented perpendicular to the plane of crack progress is generated. The fissure progress is then stabilized due to suppression of the displacement of the fissure opening because of the pulling out of the reinforcements oriented obliquely to the plane of the crack. In assessing fracture behavior, it also is relevant to consider the combination of fracture behaviors of the 3A3D and 4A3D. From the fracture photographs shown in Figure 6 [photos not reproduced] the condition of the reinforcement fractured by bending and the reinforcement that is pulled out can be seen clearly.

In contrast, the Type B test piece contains reinforcements that obliquely intersect the crack progress plane, and reinforcements that are parallel so that no unstable fissure progress can be seen, as in the Type A test piece, and there is a stable fissure growth similar to the fracture behavior of the 4A3D.

In this manner, the high degree of toughness of the 7A3D is achieved by the reinforcements after the fracture, and the pull-out of the reinforcements that are oriented obliquely. In other words, the degree of toughness is determined by the fraction of the reinforcements that can contribute to toughening and that can be pulled out.

Figure 7 shows the results of measuring the WOF values of the MA3D's. The values for the 7A3D's lie between the values for the 4A3D's, in which all of the reinforcements are oriented obliquely with respect to crack planes, and the values for the 3A3D's, in which the reinforcements are oriented in directions perpendicular to and parallel with the crack planes. Moreover, the values are larger than those for the Type B test pieces, which have a greater number of obliquely oriented reinforcements that can be pulled out.
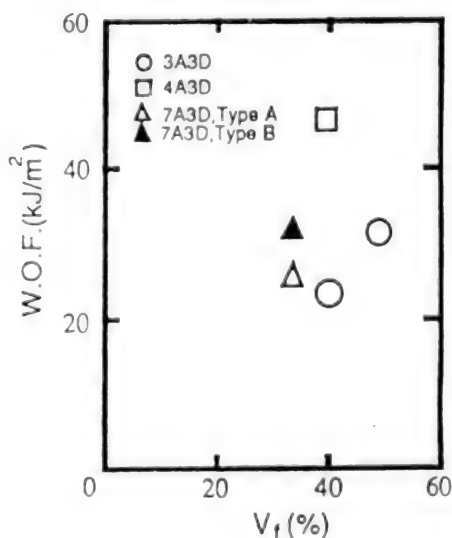


Figure 7.  WOF of MA3D's

14

The results of our theoretical analysis, which we have reported previously, show that the parameters which become important for enhancing toughness are the shape of the reinforcement and the orientation angle of the reinforcement with respect to the crack plane. The results of this experiment support our earlier conclusions, and serve to reconfirm the necessity of three-dimensional material designs.

5.   Conclusions

We examined the compressive strength and fracture toughness of seven-axial reinforced three-dimensional composites, which are multiaxial reinforced composites, based on our experimental results. A comparison with three-axial and four-axial reinforced three-dimensional composites enabled us to determine that the fracture mechanism and characteristic values depend strongly on the direction of the three-dimensional orientations of the reinforcements. The results of our study can be summarized as follows:

(1) Seven-axial reinforced three-dimensional composites make it possible to obtain three-dimensionally less anisotropic characteristics for the compressive modulus of elasticity, compressive strength, and fracture toughness. This fact suggests that it should be possible to obtain materials that have high three-dimensional specific rigidity and specific strength, and low thermal expansion through the use of high elasticity and high strength reinforcements.

(2) The mechanism of the compressive fracture and toughness enhancement depend strongly on the orientation direction of the reinforcements, and the seven-axial reinforced composites that have the reinforcement orientations of both of the three-axial and the four-axial reinforced composites showed the corresponding fracture behavior and characteristic values.

Energy Absorption of Multiaxial Reinforced 3D Composites

[Article by A. Mori, et al., Materials and Electronic Device Laboratory, Mitsubishi Electric Corporation]

[Text]  1.  Introduction

As the applications for composite materials become increasingly diverse, the necessity for three-dimensional materials development technology also is growing.  In particular, for structural materials and vibration-proof materials, methods for controlling the multiaxial stress and vibrations that are generated are required.  In three-dimensional composites, it is possible to multiaxialize the constitutional elements (reinforcements) three dimensionally, which cannot be done with conventional laminated-type composites, and we anticipate that it will be possible to absorb any factors that may be generated.

This article will discuss four-axial reinforced three-dimensional composites (4A3D's), and we will report the results of our examination of the absorption of energy due to fracture, and of the vibration characteristics.

2.  Test Material

We manufactured a four-axial three-dimensional preform, as shown in Figure 1, in which a unidirectionally reinforced CFRP rod served as the reinforcement, as shown in Table 1.  This provided the material to be served for the test. Next, a composite material was obtained by impregnating, in a vacuum, a matrix that has been given flexibility, and then curing it.  A test piece for compression and vibration tests was manufactured by segmenting a portion of the formed composite in the direction indicated by the broken line in Figure 1, which is considered to have the largest amount of deformation.

3.  Evaluation Method

3.1  Compression Test

The spring constant, modulus of elasticity, fracture strength, and energy absorption were determined from the load-displacement curve shown in

16

Figure 2.   The testing machine was a universal testing machine Model-1185
made by Instron Corporation.   Measurements were taken at a cross-head speed
of 0.5 mm/min.   The spring constant is said to be necessary in determining
the vibration characteristic in terms of the value represented by the ratio
of load/displacement in the elastic region.   Further, the amount of energy
absorption is the amount of work per unit volume applied externally to the
test piece.   This was determined by dividing the amount of work corresponding
to the area surrounded by the load-displacement curve, and the displacement
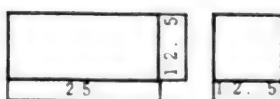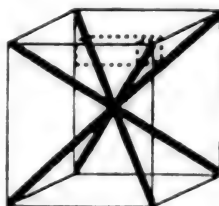axis, by the volume of the test piece.



Figure 1.   Conceptual View of Reinforcement Orientation and
            Test Piece Dimensions

Table 1.   Materials for Testing

| Reinforceme t | CFRP rod |
|---|---|
|  | Fiber: Toray M46J 3K1x4<br>Resin: General epoxy resin for drawing<br>Diameter: 0.67 mm<br>Vf: 70 percent |
| Matrix | Main agent: Bisphenol A system epoxy resin<br>Curing agent: Flexibility imparting amine |

3.2   Vibration Test

The resonance factor and the resonance frequency were determined for a test
piece similar to the one used in the compression test.   This was done by
using the vibration characteristic measuring system shown in Figure 3.   Three
test pieces were fixed with an instant adhesive on a measurement sample fix-
ing table, as shown in Figure 4, in uniform directions from the center of the
table, and a weight was fixed on top of the test pieces in the position indi-
cated in the figure.   The vibration was measured using accelerometers that
were set on the weight and on the fixing table when the table was set to
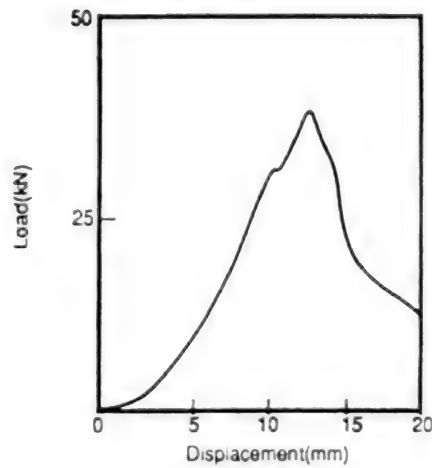vibrate.
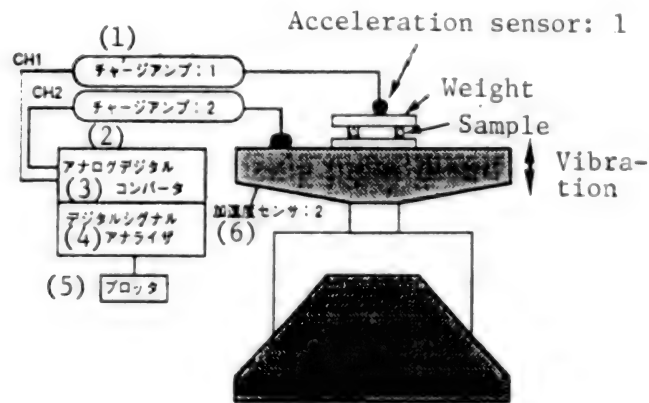
17

Figure 2.   Load-Displacement Curve for 4A3D



Figure 3.   System for Measuring Vibration Characteristics

Key:
1. Charging amplifier: 1
2. Charging amplifier: 2
3. Analog-digital converter
4. Digital signal analyzer
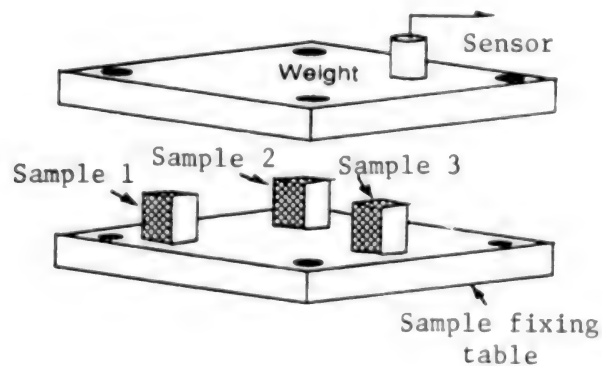5. Plotter
6. Acceleration sensor: 2



Figure 4.   Mounting Scheme of Sample for Vibration Test

18

## 4. Results and Considerations

The results for strength, modulus of elasticity, and energy absorption obtained by the compression test are shown in Table 2 for a 4A3D (N-4A3D) composite that uses a general-purpose epoxy matrix rather than a conventional laminated composite (laminated material). Although the strength and the modulus of elasticity are inferior to the sample used for comparison, the energy absorption is somewhat greater. This is believed to be due to the wider deformation range until the initial fracture, greater expansion, and greater adhesion of the matrix resin than is the case for the N-4A3D, as shown in Figure 5.

Table 2.   Comparison of Compression Characteristics
for Various Materials

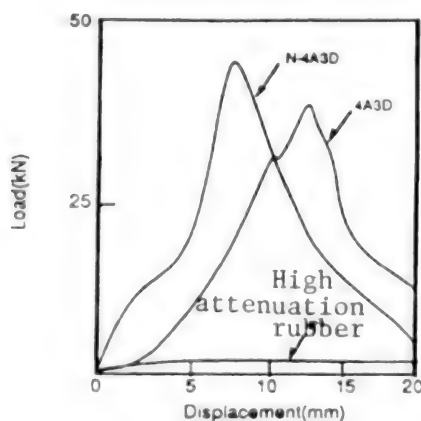| Sample | Strength (MPa) | Modulus of elasticity (GPa) | Amount of energy absorption (kJ/m$^3$) |
|---|---|---|---|
| 4A3D | 235 | 3.6 | 42 |
| 4A3D general purpose epoxy | 343 | 5.7 | 36 |
| Composite | 280 | 36 | 4 |



Figure 5.   Comparison of Compressive Fracture Behavior

The measurement results of the vibration test are shown in Figure 6. These are compared to the results for two kinds of rubber that are generally used as vibration-proof materials. The resonance magnification of the 4A3D is lower than that of the vibration-proof rubbers, indicating a considerably high attenuation effect for vibration. This leads one to anticipate that not only the matrix resin but also the three-dimensionally oriented reinforcements are affecting the attenuation of vibrations.

The ratio of the static spring constant to the dynamic spring constant obtainable from Equation 1 as a function of the resonance magnification is shown in Figure 7. It is believed that the vibration-proof effect against

19

the load (strength) is higher than that of the vibration-proof rubber for greater values of the spring constant ratio, and that the load-resistant region can be expanded accordingly.
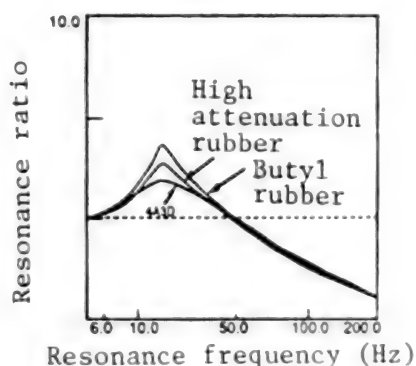


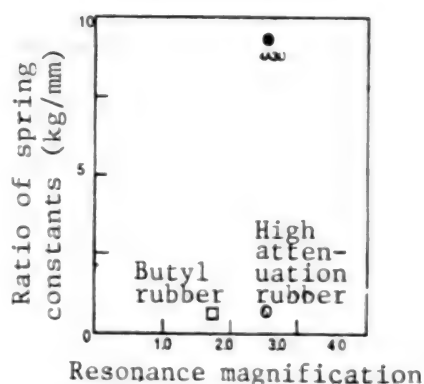Figure 6. Vibration Attenuation Characteristics



Figure 7. Relationship Between Vibration Characteristics and Spring Constants

It is interesting to note from the figure that the spring constant ratio for the 4A3D is about five times greater than those for the existing vibration-proof rubbers. At this point we made a comparison with general materials from the static as well as dynamic viewpoints. This comparison is shown in Figure 8. The loss coefficient, which can be obtained from Equation 2, gives rise to a higher attenuation effect when its value is larger, and this makes it possible to suppress the vibration transmission factor at the resonance frequency, that is, the resonance magnification. From the figure, it can be seen that the 4A3D material is better balanced in terms of both strength and vibration.

$$f = \frac{1}{2\pi}\sqrt{\frac{Kd \times G}{W}}$$

$$\eta = \frac{1}{\sqrt{\mu^2 - 1}}$$

f : Resonance frequency
W : Load
Kd: Dynamic spring constant
G : Acceleration of gravity

η: Loss coefficient
μ: Resonance magnification

Equation 2

Equation 1

## 5. Conclusions

We measured the compression and vibrational characteristics of a four-axial reinforced three-dimensional composite assembled witn the use of unidirectionally reinforced CFRP rods. We replaced the ordinary epoxy resin normally used for the matrix resin with an epoxy resin that offers greater flexibility. We found that energy absorption is increased, although strength and the elastic constant decrease somewhat, giving a vibrational characteristic

better than that of the vibration-proof rubbers. These results suggest that this material has the potential to be used as a vibration-isolating material for structural materials.
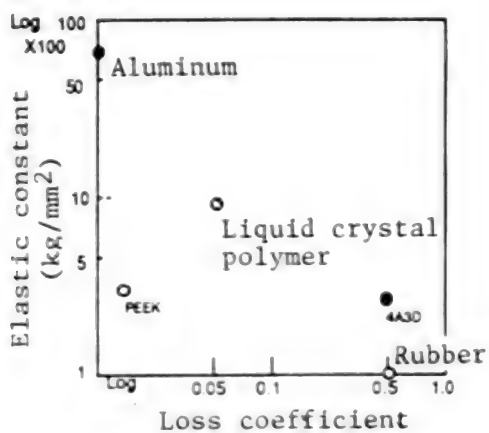


Figure 8. Relationship Between Mechanical and Vibrational Properties

Forming Processing of SiC(P)/A6061 Metal Matrix Composite

[Article by M. Agawa, et al., TYK Corporation]

[Text]  1.  Introduction

Light-weight aluminum alloys provide good heat resistance, and metal matrix composites (MMC's) obtained by adding high-hardness ceramics have excellent specific strength and specific elasticity with improved high temperature characteristics and abrasion resistance.  MMC's already are being put to practical use by the aerospace industry in the United States.  In Japan, these materials are being used for pistons and connecting rods in automobile engines, golf club heads, frames for bicycles, etc.

With regard to the ceramics used as a reinforcement material, those most frequently used are made of SiC regardless of their form, that is, whether they are fibers or whiskers.  However, as yet there have been only a few studies related to forming and processing methods, such as forging, rolling, and cutting, that can be used to make parts out of MMC's.

In the study to be reported here, we investigated the ease of disruption at various temperatures and the abrasion property of various kinds of chipping tools for lathe machining of the metal matrix composite SiC(P)/A6061.  We obtained this composite by compounding general-purpose industrial SiC particles, which are said to be costwise advantageous, and the powder of the A6061Al alloy by the hot extrusion process.

2.  Experimental Method

2.1  Manufacturing Method

The aluminum alloy used to produce the powder for our experiment is the Al-Mg-Si system alloy A6061.  The powder is classified as mesh-150 after manufacture by the gas atomizing method.  The alloy composition is shown in Table 1.  The SiC particles that serve as the reinforcement material have an average grain size of $d = 7.2$ $\mu$m.  The properties of the SiC particles are shown in Table 2.  An SEM image of the SiC particles is shown in Photograph 1 [not reproduced].  For mixing, we used a dry-type rotary ball

22

mill. The mixed powder was molded in a die to obtain a green compact of
φ50 mm x 100 mm. The forming pressure was 98 MPa, and the density ratio
was about 75 percent. We used a hot extruder to obtain a rod of φ15 mm x 1 m
from the green compact. The temperature was 843°K, and the ram speed was
2 mm/min. The appearance of the rod is shown in Photograph 2 [not repro-
duced]. The above process is shown in Figure 1. A sketch of the hot extruder
used in the experiment is shown in Figure 2. From a specimen manufactured by
this process, we formed a test piece for the disruption test and the tool
abrasion test by machining in the longitudinal direction.

Table 1. Chemical Composition of the Al Alloy (%)

| Si | Fe | Cu | Mg | Mn | Cr | Zn | Al |
|------|------|------|------|------|------|------|------|
| 0.76 | 0.51 | 0.28 | 0.96 | 0.04 | 0.21 | 0.10 | Bal. |

Table 2. Characteristics of SiC Particles

| Composition (wt%) | $\alpha$-SiC | 99 |
|---|---|---|
| | Free C | 0.4 |
| | $SiO_x$ | 0.1 |
| Particle density (g/cm$^3$) | 3.2 | |

| Weighing | → | Dry mixing | → | Molding | → | Hot extrusion |
|---|---|---|---|---|---|---|

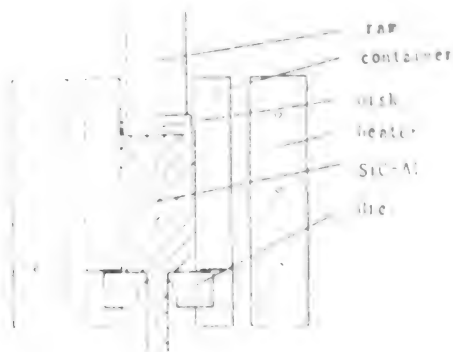Figure 1. Flow Chart of Manufacturing Process



Figure 2. Sketch of Hot Extruder

23

2.2 Measuring Method

(1) Microstructure: After polishing, the sample was subjected to vapor etching, and the structure was observed with an optical microscope.

(2) Disruption characteristic: We performed a disruption test according to the method recommended by the Plastic Processing Society of Japan in order to examine the disruption limit at various temperatures. The test, which was a compression test with constrained end faces, used a tool with concentric circles. The test temperature was conducted at four temperatures: room temperature, 150, 300, and 450°C. The test piece was machined by cutting a cylindrical test piece of $\phi14 \times 21$ mm in the longitudinal direction of the extruded rod. The limiting disruption factor was determined by the following equation:

$$\varepsilon_{hc} = \frac{h_n - h_o}{h_n} \times 100$$

$\varepsilon_{hc}$: limiting disruption factor (%)
$h_n$ : original height of the test piece
$h_o$ : height of the test piece at the time of crack generation

(3) Tool abrasion characteristic: A specimen of $\phi1.5$ mm $\times$ 200 mm was set on a general purpose lathe, and it was dry machined under the following conditions: cutting speeds = 100 and 200 m/min, notching = 0.05 mm/rev, feed = 0.1 mm/rev. For the chip shape, we used ISO specification TNMA 160408. For the chip material, we used natural diamond, compax diamond, CBN, cemented carbide, and cermet. The cutting time and the amount of wear on the chip flank caused by cutting with various kinds of chips were examined.

3. Results of Experiment and Considerations

3.1 Microstructure

The structure as observed by an optical microscope is shown in Photograph 3 [not reproduced]. No manufacturing defects, such as voids, were observed because the extrusion process was used in manufacturing.

3.2 Temperature-Limiting Disruption Factor

At room temperature and at 150°C, where the disruption limit is low, large and sharp longitudinal cracks were generated. At 300 and 450°C, fine hair cracks were seen at the center of the test piece after a sufficient plastic deformation was obtained. These results agreed with those reported by Kanetake, et al.

3.3 Cutting Time -- Amount of Chip Flank Wear

The results of the tool abrasion test are shown in Figure 4. The hardness of various kinds of chip materials, and the amounts of flank abrasion are shown in Table 3. It can be seen that continuous cutting with smaller flank

abrasion is possible for a high-hardness chip. Since the hardness of the SiC particles contained in the specimen is $H_V = 3,000$, we believe that conspicuous abrasion occurs when the hardness of the material of the chip is less than the value just mentioned.
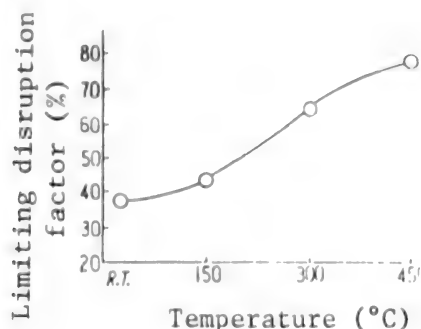
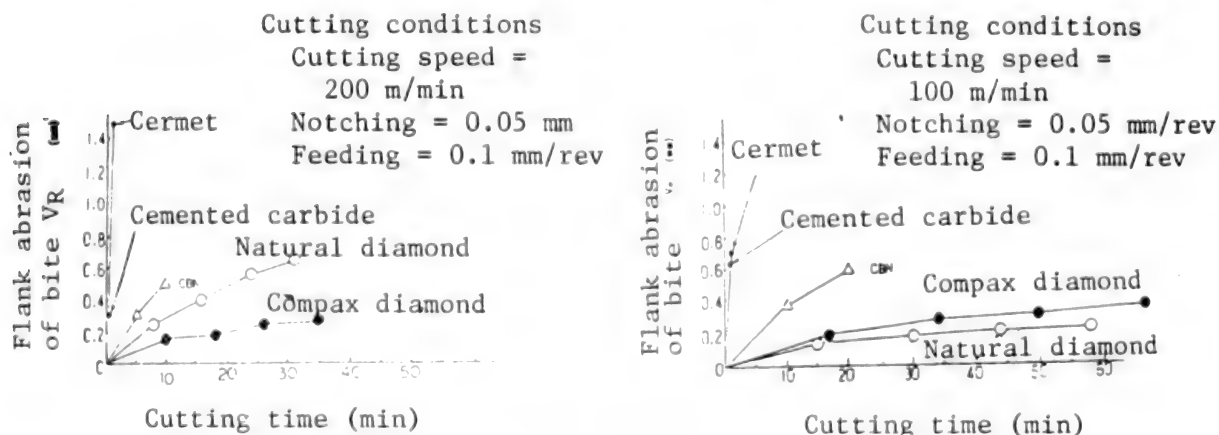

Figure 3.  Plot of Temperature-Limiting Disruption Factor



Figure 4.  Results of Tool Abrasion Test

Table 3.  Chip Hardness and Flank Abrasion Rate $V_B/T$

| Chip type | $H_V$ | Flank abrasion rate (mm/min) | |
|---|---|---|---|
| | | Cutting speed 100 m/min | 200 |
| Cermet | 1,700 | 0.7 | 0.75 |
| Cemented carbide | 1,500 | 0.65 | 0.3 |
| CBN | 3,500 | 0.03 | 0.055 |
| Compax diamond | 10,000 | 0.006 | 0.009 |
| Natural diamond | 12,000 | 0.003 | 0.02 |

4.  Conclusions

(1) Although the limiting disruption factor is less than 45 percent at room temperature and 150°C, the factor is higher than 70 percent at 300 and 450°C, and a very satisfactory ease of formation was obtained.

25

(2) Although a flank abrasion of less than 0.3 mm was obtained even after the continuation of cutting for 1 hour with natural diamond and compax diamond, a heavy abrasion of greater than 0.6 mm was obtained about 1 minute after the start of cutting with cermet or cemented carbide.

Mechanical Properties of Metal Matrix Composite SiC(P)/A6061

[Article by M. Matsushima, et al., National Aerospace Laboratory and TYK Corporation]

[Text]  1.  Introduction

Reinforcements for metal matrix composites (MMC's) include long fibers, short fibers, whiskers, particles, etc.  At present, the base materials for MMC's are primarily pure aluminum or aluminum alloys.  A highly advanced technology is required for the uniform dispersion of the reinforcement and the base material in the formation of MMC's.  Candidate methods include the hot press method, which uses preforms that are intermediate materials; the die casting method, in which the reinforcement is mixed into molten aluminum; and the drawing method.  This paper provides a systematic report about tests to measure the static strength properties, bending fatigue properties, and tensile strength in high-temperature environments, together with the results of a short cylinder compression test on a particle-dispersed MMC (SiC(P)/ A6061) manufactured by the hot extrusion method after dry mixing an atomized aluminum alloy powder and SiC particles.  In addition, a compression test using a T-shaped material was carried out as a first step toward the structural members, and we also will report the results of an evaluation of its mechanical properties.  Further, the test method will be discussed.

2.  Test Method on the Material Test Piece Level

2.1  Tensile Test

With regard to the atomized powder that serves as the base material for the particle-dispersed metallic composite, there are two basic types -- one in which the gaseous atmosphere at the time of manufacture is the earth's atmosphere, and another where this atmosphere is $N_2$ gas.  Moreover, there are two types of SiC reinforcement particles -- F (mean grain diameter = 0.44 μm) and G (mean grain diameter = 5.8 μm) depending upon the difference in the grain size distribution.  Small test pieces, like those shown in Figure 1 (1) were made from the four kinds of materials (Vf = 20 percent) obtained by varying the combination of the constituent materials.  These test pieces were used to evaluate tensile strength at room temperature.  The

27

results for the tensile modulus are shown in Table 1. For the purpose of comparison, the results of test for a sample obtained by extruding the atomized powder of the 6061 material alone is also included in the table. Similar results for tensile strength are shown in Table 2. The composite formed with an atomized powder that had been produced in the atmosphere showed a high value. Figure 2 shows the load-strain curves for the composite materials formed by combining F and G with the powder atomized in the atmosphere. The F-type sample showed a behavior pattern similar to that of the base material. The G-type sample has a high yielding stress, but the stress beyond the yielding point barely increases. However, considering the fact that the mean grain diameter of the atomized powder is 44 μm, and that problems arise from the difference in the grain diameters in the dry-type mixing process, the combination of the atmospherically atomized powder and the G-type particles, produces a good result.
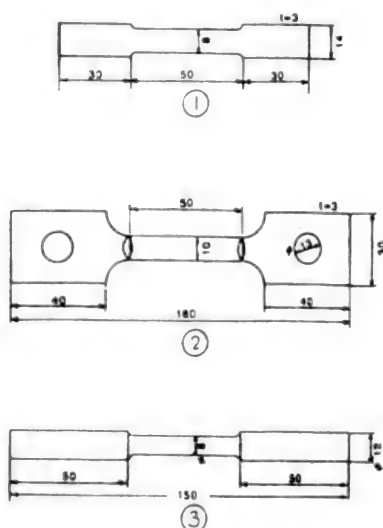


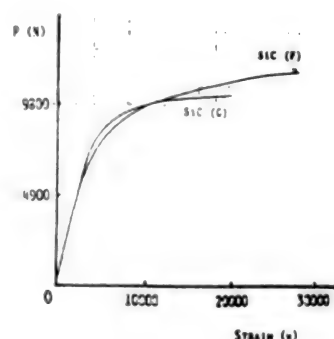Figure 1. Various Types of Tensile Test Pieces



Figure 2. Load-Strain Diagrams for F,G/A6061 (Air)

Table 1. Results for (1) Type Tensile Modulus

| Specimen | Et (GPa) | Mean |
|---|---|---|
| 6061 (A) | 79.1 – 79.6 | 79.3 |
| SiC (F)/6061 (A) | 100.9 – 101.7 | 101.3 |
| SiC (G)/6061 (A) | 104.3 – 107.0 | 105.5 |
| SiC (F)/6061 (N) | 97.8 – 99.4 | 98.6 |
| SiC (G)/6061 (N) | 101.3 – 104.0 | 102.7 |

Table 2.  Results for (1) Type Tensile Strength

| Specimen | σt (MPa) | Mean |
|---|---|---|
| 6061 (A) | 358 – 417 | 387 |
| SiC (F)/6061 (A) | 427 – 488 | 457 |
| SiC (G)/6061 (A) | 441 – 449 | 445 |
| SiC (F)/6061 (N) | 440 – 453 | 446 |
| SiC (G)/6061 (N) | 399 – 408 | 403 |

Drawing on the results described above, we performed a tensile test at a high temperature (300°C), as shown in Figure 1 (2), for the material where Vf = 20 percent.  This material was obtained by heat treating (T6) the combination of the atmospherically atomized powder and the SiC particles (G) that was selected as optimal.  The results are shown in Figure 3.  It can be seen that strength values higher than those of the base material is obtained up to 150°C.
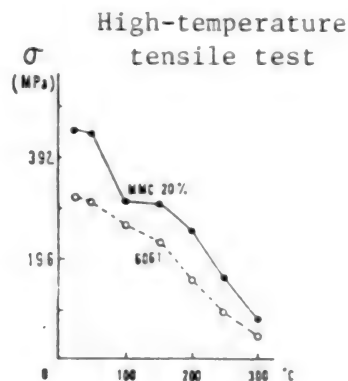


Figure 3.  Results of Tensile Test at High Temperature (~300°C) for (2) Type Sample

In addition, we performed a tensile test at room temperature using a stepped rod-shaped test piece (Figure 1 (3)) for materials where Vf = 0, 20, and 30 percent to determine the relationship between the particle content fraction, the modulus of elasticity, and strength.  The results for the modulus of elasticity are shown in Table 3, and the results for strength are shown in Table 4.  The modulus of elasticity value is generally proportional to Vf, and the strength value increased for larger values of Vf.  The anti-abrasion property increases when the particle content fraction is 30 percent, but we confirmed that there is a tendency for the degree of damage at the die port used in the extrusion formation method to become high.

2.2  Compression Test

We performed a compression test at room temperature using a short cylindrical sample of φ12 mm and 40 mm high.  We used three types whose particle content fractions were Vf = 0, 10, and 20 percent.  Since the shape of the test piece can be formed during manufacture by hot extrusion, and given that machining

of the test piece on a lathe is also possible, we were able to prepare a circular rod-type test piece. The shape of the test piece is shown in Figure 5. In particular, we needed to exercise care since the influence of the finishing condition of both end faces on the results of the experiment is large. The effects of the experiment are shown in Figure 6. The results for the modulus of elasticity are given in Table 5, and the results for strength are given in Table 6. These tests confirmed that the modulus of elasticity decreased, whereas strength was increased.

Table 3. Results for Tensile Modulus of (3) Type Sample

| Test piece | Modulus of elasticity (GPa) | Mean value |
|---|---|---|
| 6061 | 71.4 - 77.5 | 75.9 |
| MMC-20 | 100 - 113 | 111 |
| MMC-30 | 130 - 146 | 135 |

Table 4. Results for Strength of (3) Type Sample

| Test piece | Compressive strength (MPa) | Mean value |
|---|---|---|
| 6061 | 370 - 386 | 380 |
| MMC-20 | 410 - 433 | 423 |
| MMC-30 | 435 - 489 | 458 |



Figure 5. Compression Test Piece     Figure 6. Effects of Compression Test

Table 5. Results for Compression Modulus

| Test piece | Modulus of elasticity (GPa) | Mean value |
|---|---|---|
| 40L 6061 | 71.2 - 72.9 | 72.1 |
| 40L Vf=10 | 78.3 - 88.4 | 85.9 |
| 40L Vf=20 | 96.5 - 105 | 101 |

Table 6. Results for Compressive Strength

| Test piece | Compressive strength (MPa) | Mean value |
|---|---|---|
| 40L 6061 | 407 - 452 | 425 |
| 40L Vf=10 | 451 - 461 | 456 |
| 40L Vf=20 | 452 - 470 | 461 |

2.3 Bending Fatigue Test

We carried out a three-point bending test and a four-point bending test using a static bending test for the material where Vf = 20 percent. The results we obtained are comparable to those for A6061, which is the base

material.  Using a constant load-type bending fatigue testing machine (30 Hz), we carried out a bending fatigue test for a test piece like that shown in Figure 7.  The S-N diagram is shown in Figure 8.  The results of the bending test demonstrated that a fatigue strength characteristic comparable to that of the base material was obtained for the particle-dispersed MMC.  We speculate that the reason for this can be attributed to the absence of the reinforcing mechanism, as seen in the long fiber composite, at the outermost surface of the bending test piece.
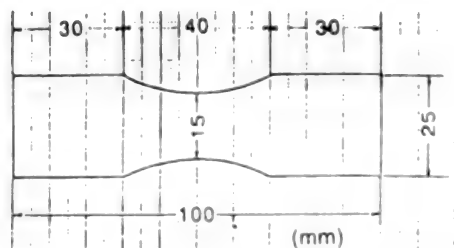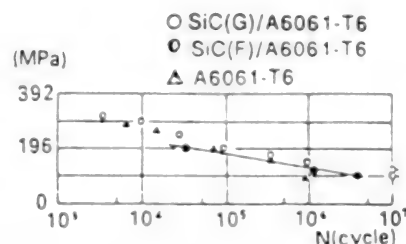


Figure 7.  Test Piece for Bending Fatigue Test

Figure 8.  S-N Diagram for Bending Fatigue Test

3.  Compression Test for T-Type Material

In the previous section, we described the characteristics of the various materials that were formed into plate- and rod-shaped test pieces.  We judged the results from an overall perspective, and decided that the best combination of a base material and a reinforcement material is that of a powder atomized in the atmosphere and SiC particles whose mean grain diameter is 7.2 μm, which are given a T6 heat treatment.  As a first step toward establishing a continuous forming technology and the application of the material to structures, we formed T-type materials that are used for basic aircraft structures by extrusion for the material system described above, and carried out a compression test at room temperature by varying the particle content fraction, Vf = 0, 10, and 20 percent.  The shape of the test piece is shown in Figure 9, and a block diagram of the test configuration is shown in Figure 10.  The test machine we used was a Model 1128 (made by Instron Corporation) with a 50-ton capacity.  We performed continuous measurement using two units of dial gauges and nine units of strain gauges.  Figure 11 [photo not reproduced] shows the testing apparatus.

4.  Results of Compression Test for T-Type Materials and Considerations

Figure 12 and Figure 13 show the load-displacement/strain diagrams for A6061 and the material where Vf = 20 percent.  Figure 14 shows the load-center displacement for the sample when Vf = 10 percent, and also the buckling load determined by the $\delta^2$ method, which is depicted by the thin line.  Table 7 shows the modulus of elasticity, final strength, and buckling stress determined by the $\delta^2$ method.  Further, Figure 15 shows the experimental values and the results of the FEM computation, depicted by the solid line.  Analogous to the results outlined in section 2.2, we believe that the test results are

significantly affected by machinability at both ends of the test piece; the initial irregularity of the test piece, in particular; and the deviation from the linearity of the web part.
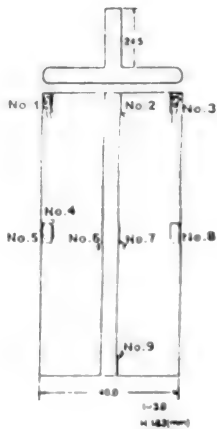


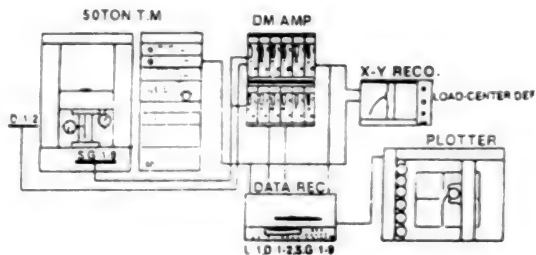Figure 9.  T-Type Compression Test Piece


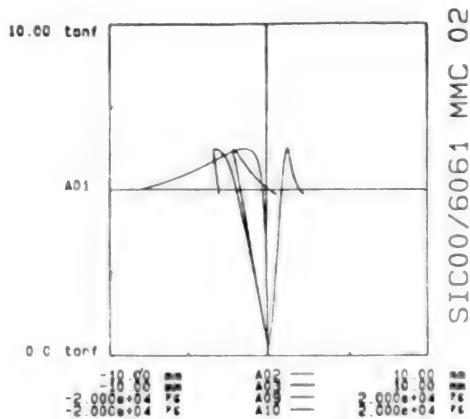
Figure 10.  Block Diagram of Test Configuration



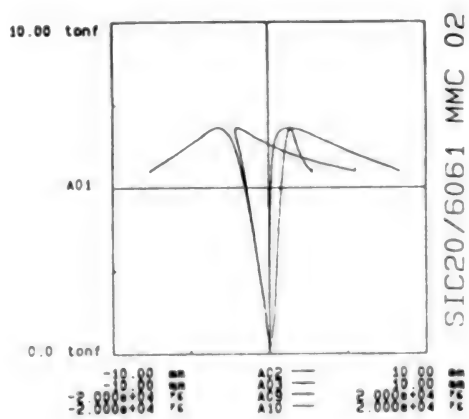Figure 12.  Load-Displacement/Strain Diagram for A6061



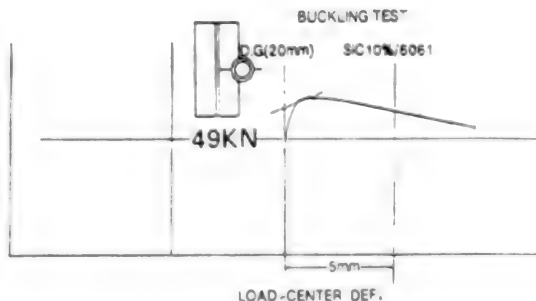Figure 13.  Load-Displacement/Strain Diagram for Sample Where Vf = 20%



Figure 14.  Load-Center Displacement Diagram

32

Table 7.   Modulus of Elasticity, Final Strength, and Buckling
Stress Determined by $\delta^2$ Method for T-Type Materials

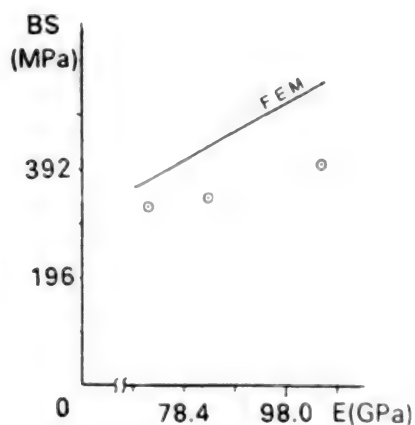|          | Ec (GPa) | S (MPa) | B · S (MPa) |
|----------|----------|---------|-------------|
| T 6061   | 71.5     | 340     | 323         |
| T Vf=10% | 83.2     | 361     | 340         |
| T Vf=20% | 104.9    | 407     | 399         |



Figure 15.   Comparison of Experimental Values for Buckling
Stress (●) and FEM Results

## 5.   Conclusions

The results of the tensile test at room temperature for the extruded single-
body material of atomized A6061 powder, the combinations of F and G SiC
particles, and powders of A and N types atomized in the atmosphere demon-
strated that the modulus of elasticity is equivalent for all combinations.
The type F sample demonstrated greater strength, but considering the manu-
facturing process, the type G sample is more promising.  Up to a temperature
of 150°C, the results were satisfactory compared to the base material.
Judging from the overall balance between the modulus of elasticity and
strength, we judge that the sample when Vf = 20 percent is best suited for
composite materials.

A compression test for T-type materials was carried out based on the above
results, and we believe that the results of this test, including the modulus
of elasticity and strength, were satisfactory for structural materials.

33

Method for Measuring Friction, Elasticity of C/C Composites

[Article by S. Sato, et al., Department of Materials Science, University of Tokyo]

[Text]  1.  Introduction

The development of carbon/carbon (C/C) composites has been making rapid progress, but quantitative measurement of the elastic modulus is extremely difficult because these materials have a complicated internal structure. Measuring techniques based on resonance vibration are advantageous in that they make it possible to easily take measurements even of materials with complicated internal structures, and to measure strain amplitude dependence and temperature dependence with a high degree of accuracy.  For this reason, we have developed a high vacuum, high temperature lateral vibration automatic internal friction device that enables one to take measurements at high temperatures.  Also, we have added the function of identifying the gaseous atoms discharged from the sample while measuring the "elastic modulus" and the "internal friction."

The purpose of this research effort was, using the device we developed, to obtain a basic understanding of material properties in limiting environments, such as those that occur in space or in a nuclear fusion reactor, by investigating the effect of temperature on the internal friction and elastic modulus of C/C composites in a hard vacuum, and to clarify their relationship with the gas discharged from the sample.

2.  Experimental Method

2.1  Apparatus

A sketch of the chamber part of our high vacuum and high temperature lateral vibration automatic internal friction device is shown in Figure 1.  The device consists of a vacuum chamber (including the sample insertion mechanism), an evacuation system, a control system, and a gas analysis system.  The samples, whose standard was set at $1^t$ x $5^w$ x $80^l$ mm$^3$, were given a wide latitude in terms of thickness (0.3-2 mm), width (2-6 mm), and length (50-100 mm).  The driving mechanism and the method for vibration detection

are of the electrostatic type, which permits continuous measurement up to a maximum of 1,000°C. Measurement is possible if a sample is electrically conductive, and even if a sample is electrically nonconductive, it can be made measurable by coating the sample surface with a conductive film. In order to carry out measurements in a clean vacuum, the measurement atmosphere was reduced to a pressure of $2 \times 10^{-5}$ Pa at room temperature and $2 \times 10^{-3}$ Pa at 800°C by means of a turbo molecular pump. A mass spectrograph is mounted on the device to identify the gases that are discharged from the surface and the interior of the sample as its temperature rises. The analyzable range of mass is 1 to 90. In addition, we were careful to design and select materials so as to reduce the background (BG) discharge of gases from the device.
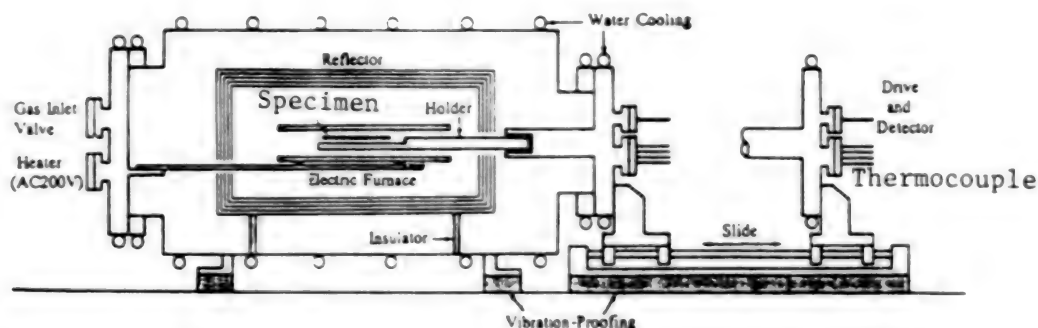


Figure 1.  Sketch of the Lateral Vibration Automatic Internal
Friction Device

2.2  Measurement of Elastic Modulus and Internal Friction

The elastic modulus (E) can be derived from Equation (1) using the resonance frequency (f):

$$E = 0.9464 \times 10^{-9} \cdot (\frac{L}{t})^3 (\frac{M}{w}) \ f^2, \qquad (1)$$

where L is the length, t is the thickness, and M is the mass of the sample.

The internal friction is determined from an analysis of the natural attenuation of vibrations. This is done by removing an external force in the state of resonance that had been produced by the external force. If one calls the amplitudes of the m-th and the (m+1)-th wave of the attenuating wave $\theta_m$ and $\theta_{m+1}$, respectively, and if the logarithmic attenuation factor at the time when the n-th amplitude is $\theta_n$ is $\delta$, the internal friction ($Q^{-1}$) is given by Equation (2):

$$Q^{-1} = \frac{\delta}{\pi} = \frac{\ln \ (\theta m / \theta n)}{\pi \ (n-m)} \qquad (2)$$

In order to remove the effect of the residual atmospheric gas at the time of measurement, the condition at the start of measurement (at room temperature) is set so that the atmospheric pressure is $7 \times 10^{-5}$ Pa.

35

## 2.3 Sample

The parameters of the C/C raw material and the matrix are shown in Table 1. The baking of the plain woven PAN system carbon fiber and the phenol resin was done in a dynamic vacuum ($10^0$-$10^1$ Pa), and the final heat treatment was given at 1,600°C. The final sample thickness was 1 mm, and an actual test piece was cut to have the dimensions of $1^t$ x $5^w$ x $80^l$ mm$^3$.

Table 1. Parameters of C/C Fiber and Matrix

| Carbon fiber | Type | Long fiber of PAN system |
|---|---|---|
| | Number of filaments | 6,000 lines |
| | Fiber diameter | 7 μm |
| | Tensile strength | 3.6 GPa |
| | Tensile modulus | 240 GPa |
| | Specific gravity | 1.77 |
| Fabric | Texture | Plain weave |
| | Surface density | 420 lines/m for both of x and y directions |
| Matrix | Phenol resin | |

## 3. Results of Experiment and Considerations

### 3.1 Internal Friction

Changes in the internal friction and the elastic modulus of C/C composites when measured continuously from 20°C to 800°C at a rate temperature increase of 3°C/min are shown in Figure 2.
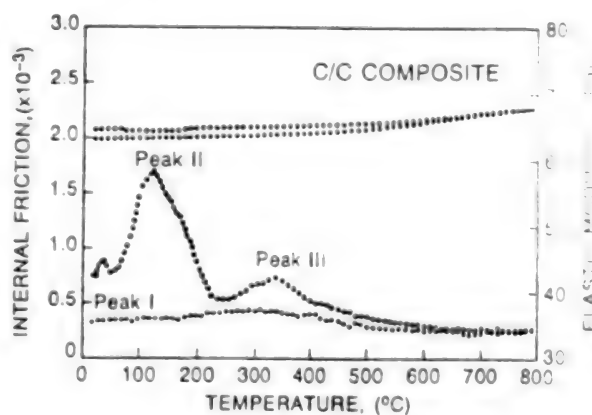


Figure 2. Relationship Between Temperature, Internal Friction, and Elastic Modulus

In the first run of the heating process, peaks in the internal friction were detected near 35°C (Peak I), 110°C (Peak II), and 340°C (Peak III). No peaks were detected at temperatures beyond 340°C. In the second run, which was performed after cooling the sample to room temperature in the furnace after completion of the first run, Peaks I to III almost disappeared. Peak I is

believed to be related to the separation of impurity atoms/molecules that had been adsorbed in the sample surface due to heating and vibration. The other two peaks disappeared due to the heat history at 800°C. This means that changes of some kind occurred in the texture or structure of the C/C composite. However, since the material we used had undergone at the time of its manufacture a final heat treatment at 1,600°C, it is hard to believe that graphitization or changes in the fine structure were in progress. This led us to think that some changes were occurring in the state of the pores or atoms of impurity gases. On these grounds we made an observation of the fine structures with an electron microscope. As shown in Photograph 1 [not reproduced], there are a number of pores, whose diameters range from several micrometers to several nanometers. The larger pores are found in locations where the matrix has a relatively large size (for example, at the so-called resin banks). The open pores (OP's) that penetrate to the surface of the sample are relatively large in size, whereas the smaller pores, which have a greater density, are observed between fibers or along fibers, forming closed pores (CP's). The internal friction is sensitive to changes in the internal structure or adsorbed atoms and molecules. Changes in the internal friction over time were measured continuously at the temperatures for Peaks II and III in order to study them in greater detail (Figure 3). It can be seen that the changes in Peak II have a saw-tooth shape that decreases gradually. We believe the mechanism that creates the saw-tooth pattern may be the discontinuous discharge of impurity gas atoms from the sample interior, and the accompanying changes in the amount of adsorbed atoms or molecules on the sample surface. This mechanism causes the pressure of the gas contained within the CP's to go up with the rise in temperature. The penetration of cracks to the CP's due to crack propagation is caused by vibrations at the time of measurement, and CP's are converted to OP's accompanied by the discharge of gaseous atoms or molecules. To confirm this, we measured the mass spectrum at the temperature of each peak to analyze the discharged gas. The results are shown in Figure 4. Masses that were detected conspicuously were at $m/e$ = 2, 12, 14, 15, 16, 17, 18, 28, and 32. Also, $H_2O$ ($m/e$ = 18) and $CO + N_2$ ($m/e$ = 28) were found abundantly in peaks II and III, respectively. The result of our investigation into the behavior of gaseous atoms or molecules discharged from a C/C composite is shown in Figure 5. Figure 5(a) shows the partial pressure of $H_2O$ vs. the measurement temperature, and Figure 5(b) shows the partial pressure of $CO + N_2$ plotted against the measurement temperature. It can be seen that Peak II, as shown in Figure 2, is not a single peak but is formed by the superimposition of subpeaks that exist in the vicinity of 160°C. Therefore, we sought to identify the subcomponents of the peak (peak decomposition) by assuming that the main peak is a single relaxation-type peak. The results are shown in Figure 6. Given the fact that the half width of Peaks I and III is too large for a single relaxation-type, and because of their shapes, we believe that these peaks correspond to the composite phenomenon of a composite peak and the separation phenomenon of gaseous atoms or molecules. Peak IIa appears at the temperature for the peak discharge of $H_2O$, suggesting that it is a relaxation-type peak caused by the discharged $H_2O$. Because Peak III appears when the sample is treated in a nitrogen environment, and because its temperature coincides with the temperature at which the amount of $CO + N_2$ discharged increases, we believe that Peak III is caused by $N_2$. Accordingly, and also taking into account the

37

fact that its temperature corresponds to the temperature at which the discharge of $CO + N_2$ in Figure 5(b) starts to rise, we believe that Peak IIb is the peak caused by CO. Peaks II and III showed little change, even when they were left standing in the atmosphere at room temperature for periods ranging from several hours to several days after measurement. This indicates that there is little adsorption and penetration of gaseous atoms or molecules into the cleaned surface and OP's. This is consistent with the decreasing behavior of Peak III shown in Figure 3, which is also supported by the measurements of gas adsorption in isotropic graphite materials.
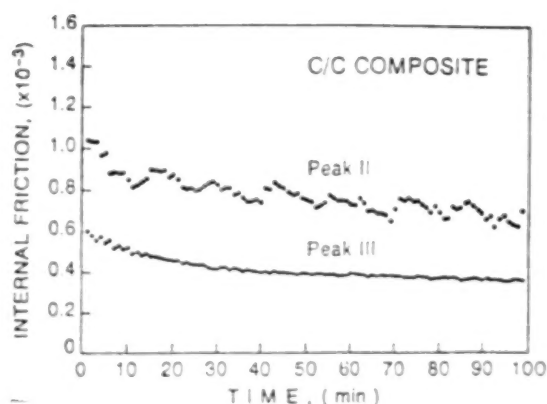


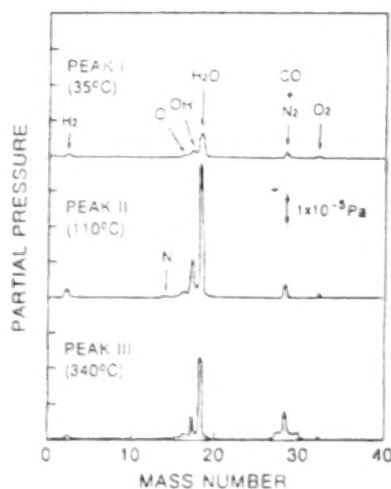Figure 3.   Changes in Internal
Friction of Peaks II and III



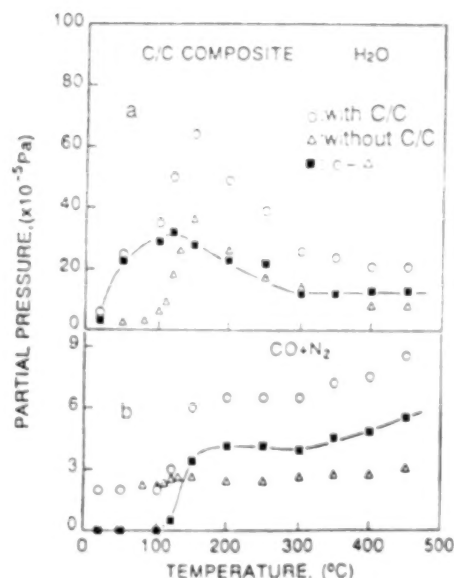Figure 4.   Mass Spectrogram at
Temperatures of Various Peaks



Figure 5.   Relationship Between
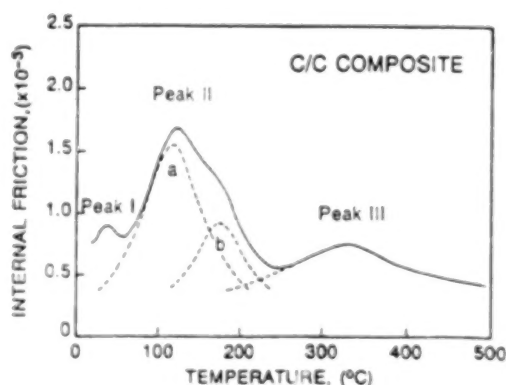Temperature and Gases Discharged
From C/C Composite



Figure 6.   Peak Decomposition of
Peak II

38

3.2  Elastic Modulus

The elastic modulus at room temperature and at a pressure of 63.5 GPa is about a quarter of the elastic modulus (240 GPa) of the fiber. This agrees well with the value anticipated from the simple compounding rule for a two-dimensional C/C composite ($V_f$ = 50 percent). The decrease in the elastic modulus in the temperature region of Peak II can be understood as the overlap of a linear decrease of the elastic modulus in a relaxation-type peak and an increase in the elastic modulus accompanying the separation of the $H_2O$ molecules. Meanwhile, the decrease in the frequency can be attributed to the influence on the vibration of the gas discharge. This discharge, in turn, is caused by the conversion of CP's to OP's due to the rise of the pressure within the CP's, and by the propagation of cracks, which is accelerated by the vibrations. That no decrease in the frequency is observed in Peak III can be attributed to the fact that it is a compounded peak, and to the problem of resolution. This agrees with the observed fact that no frequency decrease occurs in the temperature region of Peak II in the second run.

The above discussion demonstrates that differences in the various properties of the materials can be observed when measured in a high vacuum and in a different environment, even when a C/C composite undergoes heat treatment at the same temperature for equal length of time. The results presented above show that measurements taken in a hard vacuum are effective in achieving an exact evaluation of the fundamental physical properties of a material.

4.  Conclusions

1) Our measurements of the effect of temperature on the internal friction of a C/C composite revealed three peaks -- Peak I (at 35°C), Peak II (at 110°C), and Peak III (at 340°C). We believe that Peak I reflects the process whereby adsorbed materials separate from the sample surface, Peak IIa is a relaxation phenomenon due to $H_2O$, and Peaks IIb and III are peaks that accompany the discharge of CO and $N_2$, respectively.

2) As to the effect of temperature on the modulus of elasticity: We found that as temperature rises, the modulus of elasticity increases, and that the modulus of elasticity decreases according to the heating history. In addition to the fiber and the matrix, which are factors that determine the modulus of elasticity, the presence of closed pores and open pores also affects the modulus, and it is possible to interpret changes in the modulus of elasticity by analyzing the temperature dependence of the pores.

3) Our results suggest that measurement in a vacuum is an effective way to obtain the correct values of the fundamental physical properties of the materials being examined.

- END -

39

# END OF
# FICHE

# DATE FILMED

29 April 1992